Effect of N₂/TMS Gas Ratio on Mechanical and Erosion Performances of Ti-Si-C-N Nanocomposite Coatings

A.M. Abd El-Rahman, Ronghua Wei, M. Raaif, F.M. El-Hossary, M. Hammad Fawey, and M. Abo El-kassem

(Submitted February 4, 2020; in revised form April 12, 2020; published online May 21, 2020)

To optimize the tribo-mechanical performance of thick Ti-Si-CN nanocomposite coatings for a wide range of harsh industrial applications, reactive gases of nitrogen and trimethylsilane were employed with specific flow rates of PEMS process. Plasma-enhanced magnetron sputtering (PEMS) was employed for depositing thick Ti-Si-C-N nanocomposite (22-27 μ m) on Ti-6Al-4V substrates at relatively high deposition rate up to 4.5 μ m/h. Controlling the nitrogen partial pressure ratio PN₂/(PN₂ + PTMS) from 0.29 to 0.69 resulted in controlling the chemical and physical properties of the coatings. The XRD results demonstrated that the crystallinity of the nanocomposite structure increased with the increase in nitrogen pressure ratio. The coating hardness, erosion resistance, sliding wear resistance and corrosion resistance were augmented with increasing the nitrogen content in the plasma atmosphere. The results displayed that the sliding wear resistance of Ti-Si-C-N coatings increased by approximately three orders of magnitude comparing with the uncoated Ti-6Al-4V substrate. At low nitrogen content, low coefficient of friction (0.13-0.15) was achieved. Furthermore, the coating prepared at high nitrogen content reflected greater values of ratios H/E^* and H^3/E^* that correlated well with the coating erosion resistance.

Keywords corrosion, erosion resistance, nanoindentation, Ti-Si-C-N coatings, tribo-mechanical properties

1. Introduction

Ti-6Al-4V alloy is broadly applied in numerous applications such as aerospace, engine turbine, navigation and ocean examinations due to high resistance to corrosion, high toughness and high strength-to-weight ratio (Ref 1). However, the low hardness, high friction coefficient and meager wear resistance of the Ti-6Al-4V alloy limit its applications. In order to develop these properties, specific coating materials consisting of high hardness and self-lubricating can be provided. The recent addition of nanocomposite coatings in hard coating studies is destined to provide surfaces with more desired properties and functions for harsher industrial applications, in which intense power, high speed and high efficiency are increasingly inquired (Ref 2, 3). Among these nanocomposites, Ti-Si-N and Ti-Al-Si-N are considered because of their super hardness, high oxidation resistance and immovability to corrosion as well as excellent thermal stability (Ref 4-9). Moreover, the nanocomposite coatings of Ti-Al-Si-C-N and Ti-Si-C-N with surplus amounts of carbon exhibit further reduced in friction coefficient and wear (Ref 10-12). Various physical

A.M. Abd El-Rahman, Physics Department, Faculty of Science, Sohag University, Sohâg 82524, Egypt; and Mechanical and Materials Engineering Division, Southwest Research Institute, 6220 Culebra Road, San Antonio, TX 78238; Ronghua Wei, Mechanical and Materials Engineering Division, Southwest Research Institute, 6220 Culebra Road, San Antonio, TX 78238; and M. Raaif, F.M. El-Hossary, M. Hammad Fawey, and M. Abo El-kassem, Physics Department, Faculty of Science, Sohag University, Sohâg 82524, Egypt. Contact e-mail: mraaif@daad-alumni.de.

vapor deposition (PVD) techniques were successfully developed to synthesize Ti-Si-C-N nanocomposite coatings including hybrid deposition (Ref 11), cathodic arc plasma evaporation (Ref 13) and magnetron sputtering (MS) (Ref 14). Recently, Plasma-enhanced magnetron sputtering (PEMS) technique was developed as an enhanced version of the MS process in order to achieve thick coatings (> 20 µm) with high mechanical, high adhesion with substrate and tribological performance (Ref 15-17). The Ti-Si-C-N nanocomposite coatings are a promising material, which demonstrated good tribological, good corrosion resistance and corrosion performance. Ma et al. (Ref 18) synthesized Ti-Si-C-N super hard coating by (PECVD) technology with different carbon contents using gaseous mixture of TiCl₄/SiCl₄/N₂/H₂/CH₄/Ar. It was verified; the presence of nanoparticles as self-lubricating in the microstructure of super hard Ti-Si-CN coatings reduced the friction coefficient. Wei (Ref 15) demonstrated that Ti-Si-C-N nanocomposite coatings by PEMS offered excellent mechanical and tribological properties. In addition, the use of TMS gaseous as a source of Si verified great advantages including higher deposition rate, uniform elemental distribution and the more easily tuning of the composition of the coating than using solid Si target. Wang et al. (Ref 19) investigated the tribo-corrosion performance of Ti-Si-C-N coatings that achieved by arc ion plating with diverse carbon contents under artificial seawater. It was achieved low wear rates accompanying with the formation of lubricious graphite layer and maximized hardness at an optimum value of carbon content. Abd El-Rahmen et al. (Ref 20) deposited Ti-Si-CN at higher power densities and reported excellent corrosion resistance. Thick coatings are required for components that are used in severe abrasive environments such as compressor blades for aero-engines, or cylinder liners for mud pumps and valves for the oil and gas industry.

The present work is a part of a series of experiments to control the microstructure and accordingly the tribo-mechanical characteristics of the Ti-Si-C-N coatings that can be employed in a wide range of industrial sectors. To achieve durable Ti-Si-

C-N nanocomposite coatings for long-service tribo-mechanical tools and harsh applications, effective deposition parameters in PEMS should be controlled in the coating recipe. Among these parameters, the substrate power density was adjusted by controlling the ion flux and the bias voltage with the objective of synthesizing high-quality Ti-Si-C-N coatings in terms of structural, mechanical, erosion and corrosion properties (Ref 20). Moreover, Lin et al. (Ref 21) employed the same technique with varying the flow rates of hexamethyldisilazane (Si source) and C₂H₂ (C source) to develop low-friction Ti-Si-CN nanocomposite for piston ring applications. Therefore, more efforts were presented in the current work to govern the microstructure and the tribo-mechanical characteristics of the Ti-Si-C-N coatings for a wide range of similar industrial applications. The reactive gases flow rates, namely nitrogen and trimethylsilane, were controlled to achieve superior mechanical and lubrication properties. Moreover, the effect of gas flow rate on erosion and corrosion resistance for Ti-Si-C-N nanocomposites was evaluated.

2. Experimental Details

Ti-6Al-4V coupons (25 mm \times 25 mm \times 3 mm) with high purity of 99.6% (ASTM B381 grade 5) were used as the substrates for the growth of Ti-Si-C-N nanocomposite. The Ti-6Al-4V substrates were polished with SiC grit to attain final surface roughness of < 50 nm. The samples were washed in isopropyl alcohol using an ultrasonic cleaner and then introduced in the PEMS system. Ti-Si-C-N nanocomposite coatings were synthesized by sputtering of titanium from two magnetrons (15 cm in diameter) in an Ar-N₂-TMS gas mixture. Details about the PEMS process can be found elsewhere (Ref 15). In brief, the PEMS deposition process is based on the magnetron sputtering (MS) with adding global plasma. The global plasma was engendered by heating tungsten filaments with an AC power supply to initiate electrons. Moreover, the filaments were biasing with a DC discharge power supply to direct these electrons to the chamber walls. Owing to the ionizations by electron-Ar collision, the "global plasma" is produced. In the current study, the base pressure of the deposition process was approximately 7×10^{-6} mbar in all experiments. The Ar flow rate of 150 sccm was used, and the chamber pressure was 3.4×10^{-3} mbar. Before introducing the reactive gases and establishing the deposition process, the substrates were sputter cleaned with Ar-ions from the global plasma at 120 eV and 5 mA/cm² for 90 min. At this time, the magnetrons were not turned on. The substrate temperature reached to ~ 400 °C by the effect of the ion bombardment. After sputter cleaning of the samples for 60 min, the magnetrons were turned on at 500 W to sputter clean the Ti target for 30 min. Both the sample and the target cleaning processes were applied to ensure the removal of the adsorbents and surface residual oxides. Right after the cleaning processes of both the substrate and the targets and without interrupting the global plasma, the shutters of the magnetrons were opened and a titanium layer (about $\sim 4 \mu m$) was deposited as a bonding layer on the Ti-6Al-4V substrates at a bias voltage of 100 V and an applied magnetron power of 4 kW. Finally, the reactive gases were gradually introduced into the vacuum chamber for the formation of the Ti-Si-C-N coating. Then, the bias voltage was gradually reduced to 40 V, and the samples were deposited

for 6 hours for all tests. In the present work, Ti-Si-C-N nanocomposite coatings were deposited at different nitrogen partial pressure. The N_2 gas flow rate was varied from 45 sccm to 55 sccm. Then, trimethylsilane ([CH $_3$] $_3$ SiH $_4$, TMS) was introduced into the deposition chamber by a gas flow rate ranging from 12 to 15 sccm. The final working gas pressure was $3.88 \pm 0.04 \times 10^{-3}$ mbar. Consequently, Ti-Si-C-N nanocomposite coatings of different compositions could be obtained. For simplification, the nitrogen partial pressure ratio in the reactive gas mixture will be expressed by $PN_2/(PN_2 + PTMS)$ as a preparation parameter to correlate with the coatings composition and properties. Detailed preparation conditions are summarized in Table 1.

The specimens were tested and characterized engaging varieties of techniques. XRD utilizing Cu-Kα radiation was employed to distinguish the phase chemical compounds in the Ti-Si-C-N coating. The surface and cross-sectional morphology of the Ti-Si-C-N coatings were scrutinized by SEM. The adhesion of the coatings was explored by Rockwell hardness indentation test using conical diamond indenter at a testing load of 150 kg. The deformed indentation area was examined by SEM. The hardness and elastic modulus of the Ti-Si-C-N coatings were assessed by nanoindenter (MTS) at a maximum load of 300 mN to obtain the load-unload curve. To ensure the accurate results for the surface hardness and elastic modulus, at least ten measurements were taken for each sample. The values of H/E^* (the elasticity index) and H^3/E^{*2} (the resistance to plastic deformation) were calculated. The surface roughness of the Ti-Si-C-N nanocomposite coatings and substrates were measured with a soft contact profilometer (Tylor Hobson Ltd., Form Talysurf Intra 50, and UK). The diamond stylus was moved across the sample surface under a constant pressure with a cutoff value of 5 mm. The average Ra was calculated by considering five measurements for each sample. The wear rate and friction coefficient were estimated using ball-on-disk tribometer (manufacturer by CSM Instruments model TRIB-OMETER TRB) at sliding speed of 20 mm/s with applied load of 5 N (linearly reciprocating ball-on flat sliding wear). Figure 1 illustrates the schematic diagram of the ball-on-disk tribometer tester, which was utilized in this work. A 6-mmdiameter Al₂O₃ ball (TCP-C-AA-0063,

CSM, Switzerland) was used as a counterpart against the coated and uncoated Ti-6Al-4V without lubrication. The working temperature was $T=25\pm3$ °C, and the relative humidity was 30%. Three wear measurements on the surface of each sample were implemented, and the friction coefficient was recorded incessantly using a force sensor. The wear loss volume was determined by investigating the cross-sectional area of the wear track using a stylus profilometer. Multiplying the average of three-profile area by the length of the wear track, the wear volume loss can be determined. Multiplying the wear volume loss by the total sliding distance, the wear rate can be obtained.

Solid particle erosion (SPE) tests were executed using an erosion media of Al_2O_3 powder with particle size of approximately 50 μ m. The test was carried out at two impingement angles (30° and 90°), while the ambient temperature was 25 °C. The backpressure of the nozzle was 1379 mbar, producing particle velocity of 14 m/s and an erodent flow rate of 5.19 g/min. The distance between the nozzle and the tested specimens was 1 cm. The volume loss of the investigated specimens was assessed by weighting the samples before and after test with a highly precision microbalance of 0.01 mg. The erosion rate was

Table 1 Deposition conditions for Ti-Si-C-N coatings by plasma-enhanced magnetron sputtering

Sample no.	N ₂ fraction PN ₂ / (PN ₂ + PTMS), %	TMS fraction PTMS/ (PN ₂ + PTMS), %	Nitrogen flow rate, sccm	TMS flow rate, sccm	Coating thick, µm	Depos. rate, µm/h	Crystallite size, nm
QL-13	0.29	0.71	45	12	27.1	4.5	4.3
QL-14	0.45	0.55	50	12	24	4	3.8
QL-15	0.69	0.31	55	12	22.5	3.8	4.6
QL-16	0.63	0.37	55	15	21.8	3.6	4.3

Base pressure = 7×10^{-6} mbar PAr = 3.42×10^{-3} mbar (working gas pressure after introducing 150 sccm Ar gas)

Final working gas pressure (PN₂ + PTMS) $\approx 3.88 \pm 0.04 \times 10^{-3}$ mbar

PN2 working gas pressure after introducing N2 gas

PTMS working gas pressure after introducing TMS gas

Bias voltage 40 V Discharge current 5 A Deposition time 6.0 h

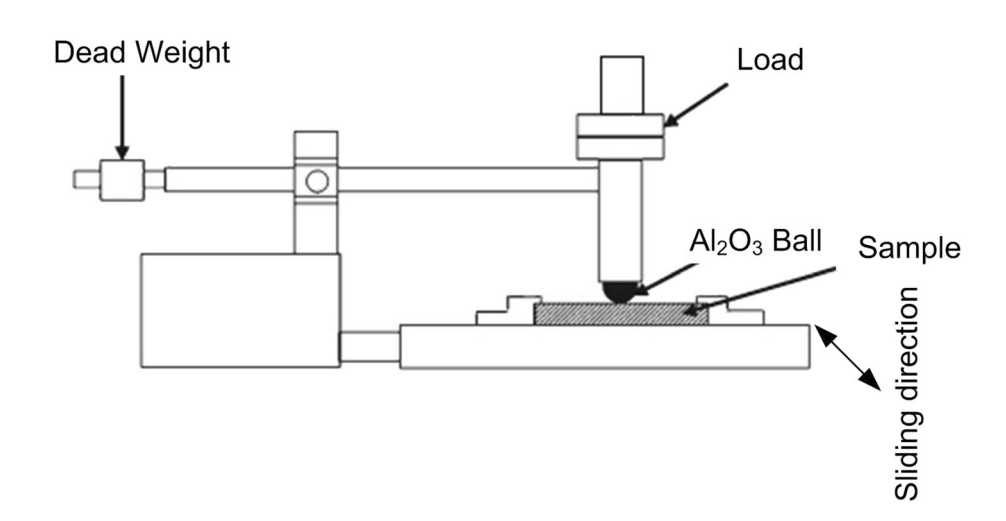


Fig. 1 Schematic diagram of the ball-on-disk tribometer tester

thus obtained by considering the previous data. The corrosion performance of the Ti-Si-C-N coatings was implemented in NaCl solution (1.0%) using Gill AC instrument. The corrosion test was executed using three electrodes; the scrutinized sample as working electrode, platinum electrode as counter and silversilver chloride saturated electrode as reference electrode. The effective corrosive area was fixed at 0.36 cm², and the test was run at temperature of 23 ± 3 °C and humidity of 36 ± 5 %. The open circuit potential (OCP) was monitored for 1 h; then, the potentiodynamic scan was performed at a rate of 0.1 mV/s.

3. Results and Discussion

3.1 Microstructure, Composition and Morphology

The X-ray diffraction patterns of the deposited Ti-Si-C-N coatings at different nitrogen gas pressure ratios $PN_2/(PN_2 + PTMS)$ are presented in Fig. 2. It can be observed that the crystalline microstructure of all Ti-Si-C-N coatings mostly consisted of $TiC_{0.3}N_{0.7}$ (JCPDS: 42-1488) which is might be overlapped with TiN (JCPDS: 38-1420). It was reported for Ti-Si-C-N-deposited utilizing TMS, the $TiC_{0.3}N_{0.7}$ and TiN sometimes were mixed with TiC, or others form the typical microstructure of Ti-Si-C-N (Ref 15, 16). The same random

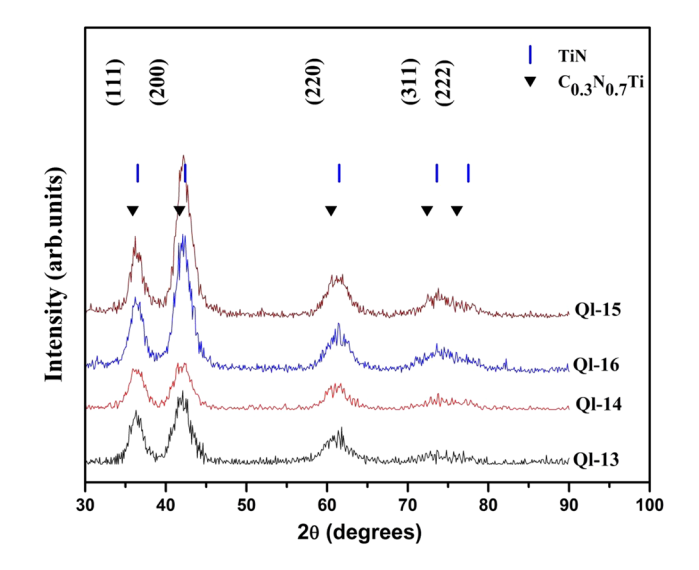


Fig. 2 X-ray diffraction patterns of Ti-Si-C-N coatings prepared at different $PN_2/(PN_2 + PTMS)$

orientations of (111), (200), (220), (311) and (222) were typically observed in the previous work from similar Ti-Si-C-N coatings (Ref 9). The absence of any silicon-based crystalline structure indicated that the Si exists in amorphous phase (s) as

a-Si₃N₄, a-Si₃C₄ (Ref 9, 11, 22), and/or a-SiC_xN_y (Ref 15, 16). Generally, it was noticed, the peak intensities increased with increasing the nitrogen gas ratio. The XRD pattern of QL-15 coatings prepared at relatively high nitrogen gas ratio (69%) exhibited the highest peak intensity among all coatings. The crystallite size calculated from Scherrer equation recorded values around 4 nm for all investigated samples and tabulated in Table 1.

EDAX was used for the quantitative analysis of the composition. Figure 3 shows the atomic concentration of titanium (Ti), silicon (Si), nitrogen (N) and carbon (C) as a function of $PN_2/(PN_2 + PTMS)$. It is demonstrated from the figure that the nitrogen is increased while the silicon is decreased with the increase in the nitrogen partial pressure ratio. The higher silicon content detected in the Ti-Si-C-N coatings deposited at low nitrogen content may be reflected in the variation in amorphous-to-crystalline phase ratio of the nanocomposite coatings. These results are correlated well with the XRD analysis (Fig. 2) which depicted the formation of lower intensities of crystalline phases ($TiC_{0.3}N_{0.7}$ or TiN) with coatings prepared at lower nitrogen content.

Figure 4 illustrates the surface (left hand) and crosssectional morphology (right hand) of Ti-Si-C-N nanocomposite prepared at $PN_2/(PN_2 + PTMS) = 0.69$. The surface morphology of the coating is characterized by a stone or cauliflowerlike structure that is densely packed with well-defined grains over the surface. Furthermore, the surface morphology is completely free from any micro-cracks or surface defects, indicating the high quality of the coatings, which can be used in intensive load and harsher applications. The cross section reflected a homogeneous band of nearly uniform thickness. Similar features were observed in the surface and the crosssectional morphology of the other coatings deposited at different gas ratios. From the cross-sectional SEM image, the coating thickness was measured and the deposition rate was calculated and is presented in Table 1. As can be observed, thick coatings (22-27 µm) were obtained at a high deposition rate of $3.6-4.5 \mu m/h$.

It is noted that the thickness and hence the deposition rate of the coatings decreased with the increase in nitrogen gas ratio (see Table 1). It is well known that increasing the nitrogen gas

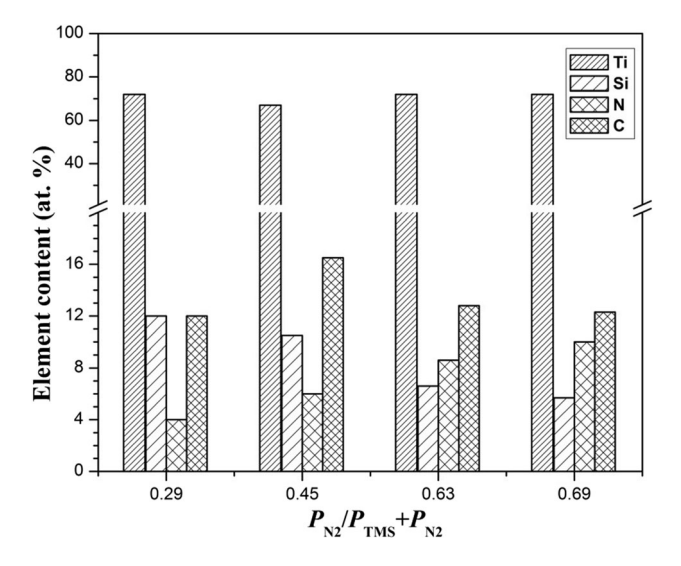


Fig. 3 EDAX analysis of Ti-Si-C-N coatings prepared at different PN₂/(PN₂ + PTMS)

fraction reduces the deposition rate due to the nitrides coverage the targets. This phenomenon is commonly called target poisoning (Ref 11, 23-28). The average surface roughness (Ra) for Ti-Si-C-N coatings as a function of nitrogen partial pressure ratio $PN_2/(PN_2 + PTMS)$ is plotted in Fig. 5. It is obvious that the average surface roughness decreased with the increase in the nitrogen partial pressure ratio. It is well known that the growth process of metallic or ceramic coatings is mainly influenced by the processing parameter and one of them is the ion-to-atom ratio (Ref 11, 29-35). At high ion-to-atom ratio, the coating becomes dense with low surface roughness. In the current study, the ion flux was nearly constant for all experiments. Even though the magnetron power was the same for all tests, the deposition rate decreased with the increase in the nitrogen gas flow ratio due to the "target poisoning effect." As a result, the ion-to-atom ratio increased and the surface roughness decreased. The obtained results were similarly reported previously. The higher the values of the deposition parameters including reactive gas flow rates (N2, TMS), ion current density and ion energy resulted in better microstructure and roughness of the coatings (Ref 28).

3.2 Coating Adhesion and Mechanical Properties

The adhesion of Ti-Si-C-N coatings was measured using a Rockwell indentation test at a load of 150 kg and classified according to VDI guidelines 3198 (1991) (Ref 36). As shown in Fig. 6, all Ti-Si-C-N coatings except the sample QL-14 reflected good adhesion with the substrate and indexed as HF1 of Daimler-Benz adhesion quality ranking. The coating for the sample QL-14 is characterized by HF2. A HF1 ranking indicates the strongest interfacial bonding between the hard coating and the metal substrate, while HF2 ranking still indicates a good adhesion even though some observed delamination around the indentation edge, and it is still sufficiently good for most applications (Ref 37). The relative low adhesion of sample QL-14 compared to all other samples is probably ascribed to the decreased nanocrystallites, or increased amorphous phase. For samples QL-13, QL-15 and QL-16, fine ring cracks were formed concentrically inside all indents, while linear cracks were formed radially outside the craters after the heavy load indentation tests that indicating the excellent adhesion of these coatings. The good adhesion is mainly attributed to the properties of the nanocomposite structure synthesized by the PEMS technology and additionally to the internal stress reduction between the tough coatings and the ductile metallic substrate that was released by the Ti-bond layer (Ref 38, 39).

The mechanical properties of Ti-Si-C-N coatings deposited at different $PN_2/(PN_2+PTMS)$ ratios were investigated using a nanoindentation test method. Figure 7 shows the load vs. depth curves of the Ti-Si-C-N coatings deposited at different $PN_2/(PN_2+PTMS)$ ratios. It is observed that the final indentation depths ($<1~\mu m$) for all coatings are far less than the coating thickness ($>20~\mu m$). Therefore, the measured surface hardness can represent the coating hardness. The elastic modulus and hardness were assessed from the load–depth curves employing the Oliver and Pharr method (Ref 40, 41). Figure 8 represents the variation in nanohardness (H) and elastic modulus (E) for the coatings prepared at different nitrogen partial pressure. The surface nanohardness and elastic modulus for the substrate recorded nearly 5 and 150 GPa, respectively. It is noted from Fig. 8 that the surface nanohardness and elastic

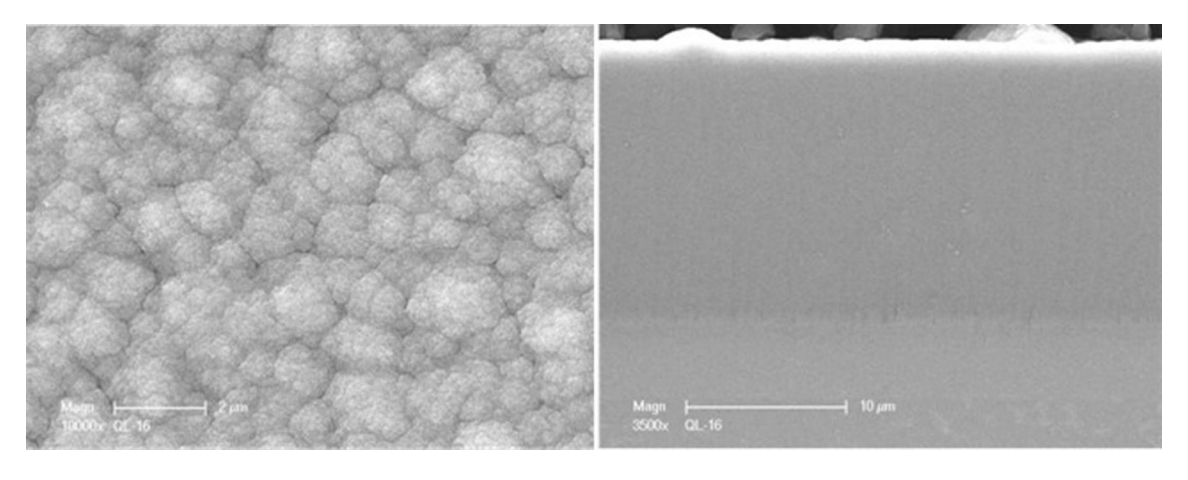


Fig. 4 Surface and cross-sectional morphology (SEM images) of Ti-Si-C-N nanocomposite coatings prepared at PN₂/(PN₂ + PTMS) = 0.71

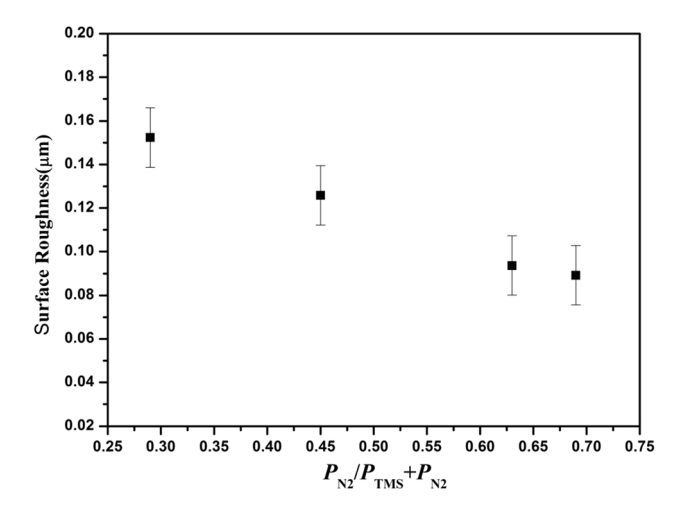


Fig. 5 Effect of PN₂/(PN₂ + PTMS) on coating surface roughness

modulus for Ti-Si-C-N coatings prepared at higher nitrogen content (QL-15 and QL-16) are higher than those deposited at lower nitrogen contents (OL-13 and OL-14). Higher hardness and elastic modulus are ascribed to the changes in the chemical composition and microstructure of the coatings. The values of H/E^* and H^3/E^{*2} , where E^* is the effective Young's modulus = $E/(1 - v^2)$ and v is the Poisson's ratio, are considered as more reliable mechanical parameters than the values of H and E for characterizing the mechanical and tribological performance of hard coatings (Ref 42-45). The results are plotted in Fig. 9, where v = 0.25 for calculating E^* . It is clear that both values of H/E^* and H^3/E^{*2} gradually increased with increasing the nitrogen partial pressure. It was observed that the higher values of H/E^* and H^3/E^{*2} the greater fracture toughness and resistance to plastic deformation (Ref 42-44, 46). Additionally, depositing the coatings at high nitrogen gas ratio contributed also in increasing the coating hardness and affected the coating adhesion to the substrate (Ref 47).

3.3 Tribological Performance

Figure 10 illustrates the coefficient of friction variations with the sliding distance for the Ti-Si-C-N coatings prepared at different partial pressure ratios PN₂/(PN₂ + PTMS). The specimens were tested using applied load of 5 N and at a sliding distance of 60 m. As observed, there is an initial running-in

stage of the wear process up to a distance of ~ 10 m. It was reported that the coating characteristics including surface roughness, hardness, adhesion and microstructure play fundamental roles in the friction and wear performances (Ref 48-50). It was clarified that the initially low COF of TiN is associated with the surface roughness and chemical reactivity at the interface between the ball and the tested sample (Ref 51). Further, the initial inconformity between the surface of the coatings and the surface of the ceramic ball leads to irregular COF in the beginning of the wear process (Ref 52). After the running-in stage, the average COF of the Ti-Si-C-N coatings prepared at lower nitrogen partial pressures (QL-13 and QL-14) has lower value than the coatings prepared at higher nitrogen partial pressures (QL-15 and QL-16). The high COF in the samples with high nitrogen pressure (QL-15 and QL-16) is ascribed to the high hardness of the wear particles that act as an abrasive in the contact surface. It should be mentioned that the higher TMS flow rate resulted in higher carbon concentration in the film which in turn led to lower COF. The lowest friction coefficient of 0.13 ± 0.000416 was observed for QL-14 that is mostly assigned to the highest carbon content ($\sim 16.7\%$). The low COF in the samples with low nitrogen pressure (QL-13 and QL-14) is related to producing fine wear debris during friction process, which act as self-lubricating debris on the rubbing surface (Ref 19). Moreover, the increase in the temperature in the interface contact leads to softening and reorientation of the self-lubricating layer (Ref 53). A. Abd El-Rhamman et al. (Ref 54) investigated COF and recorded values of 0.37 and 0.22 for Ti-Si-C-N nanocomposite deposited by CMS and PEMS, respectively, on Ti6Al4V substrate. Moreover, the wear rate Ti-Si-C-N prepared by CMS was $\sim 8.73 \times 10^{-6}$ mm³/N m and Ti-Si-C-N prepared by PEMS was recorded $\sim 6.26 \times 10^{-6} \text{ mm}^3/\text{N m}$.

The sliding wear rate of Ti-Si-C-N coatings at different nitrogen partial pressure in comparison with the uncoated Ti-6Al-4V substrate is shown in Fig. 11. The results indicated that the wear resistance of the Ti-Si-C-N coatings is improved by more than three orders of magnitude as compared to the uncoated substrate. All coatings have similar values between 1.6×10^{-7} and 9.9×10^{-7} mm³ N⁻¹ m⁻¹ that cannot be correlated well with the processing conditions. Moreover, the wear grooves were too small for the coated samples to obtain an accurate measurement for ranking these coatings. The decrease in the wear rate is related to the formation of self-lubricating layer. This layer reduces the shear strength at the contact point

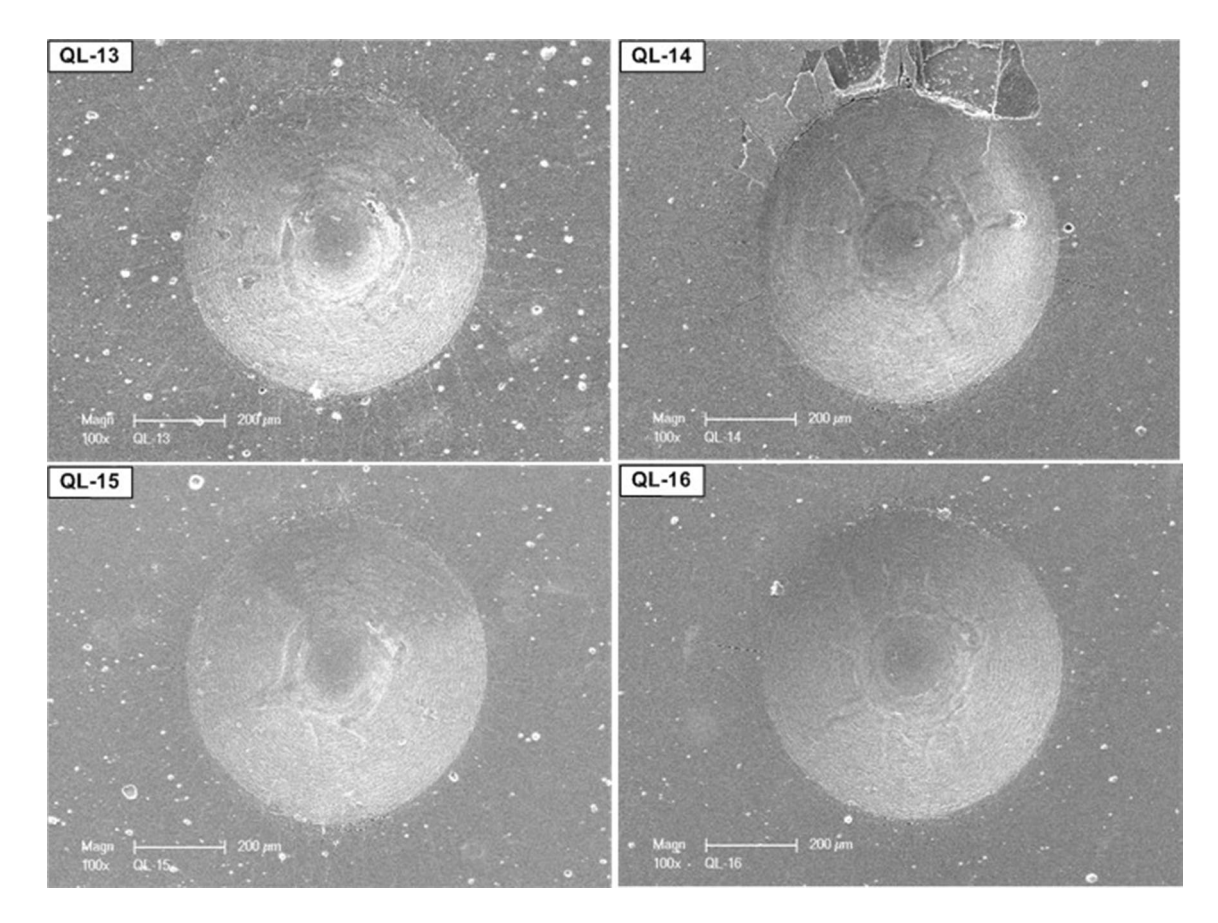


Fig. 6 Effect of PN₂/(PN₂ + PTMS) on coating adhesion test using Rockwell C-scale indentation at 150 kg load

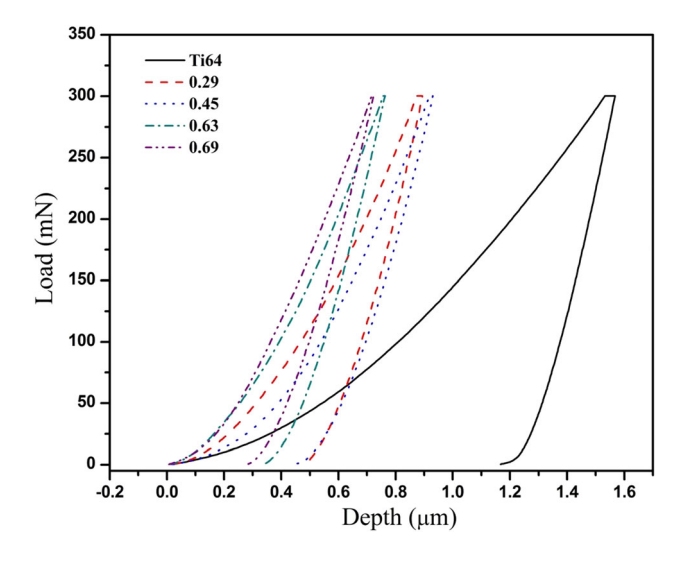


Fig. 7 Nanoindentation load–depth curves as a function of $PN_2/(PN_2 + PTMS)$ for Ti-Si-C-N nanocomposite coatings

and presented smoother contact surfaces in dry sliding conditions (Ref 55). Moreover, the increase in the temperature in the rubbing surfaces with time results in sintering of fine wear debris particles, which form self-lubricating layers. Furthermore, the increase in temperature leads to the increase in the oxidation rate and the formation of oxide layers resulting in smoother interface layer contact (Ref 55). This result is in line with the observations for the nanostructured composite coatings

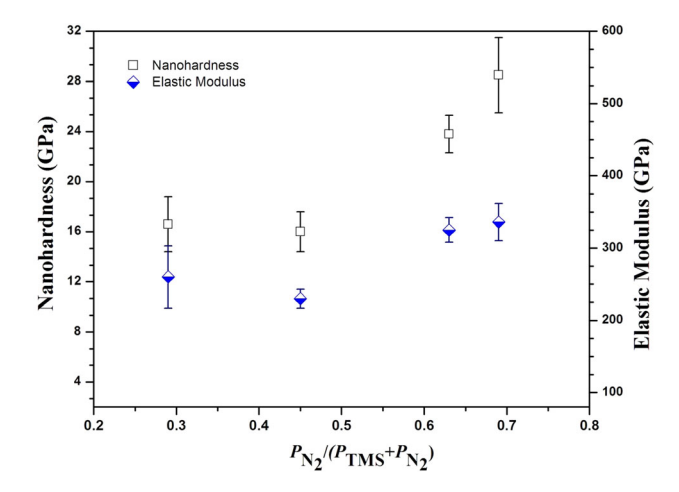


Fig. 8 Effect of $PN_2/(PN_2 + PTMS)$ on coating nanohardness and modulus of elasticity

that have an excellent sliding wear resistance (Ref 18, 44, 46). M. Abedi et al. (Ref 56) deposited Ti-Si-C-N by PECVD on AISI H13 at both 350 and 500 °C. The lowest COF of 0.1 for the specimen deposited at 350 °C and then annealed at 500 °C was reported. The reduction in COF is attributed to the accumulation of wear carbon particles during dry sliding which act as solid lubricant. Wear rates of 1.9×10^{-5} mm³/Nm for the coating at 350 °C and 6.68×10^{-6} mm³/Nm for the coating at 350 °C and then annealed at 500 °C were reported. It

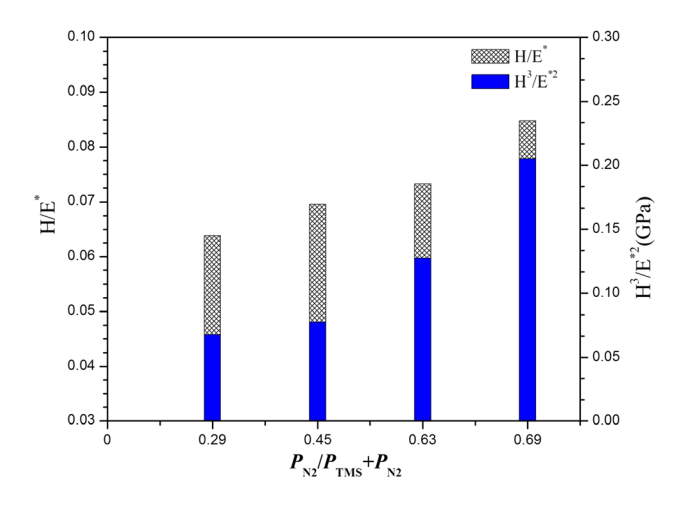


Fig. 9 Effect of $PN_2/(PN_2 + PTMS)$ on H/E and H^3/E^{*2} of Ti-Si-C-N nanocomposite coatings

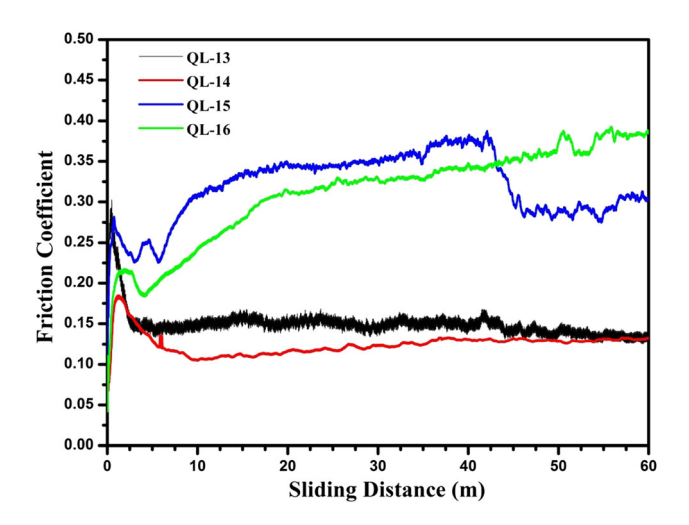


Fig. 10 Effect of PN₂/(PN₂ + PTMS) on coefficient of friction of Ti-Si-C-N nanocomposite coatings

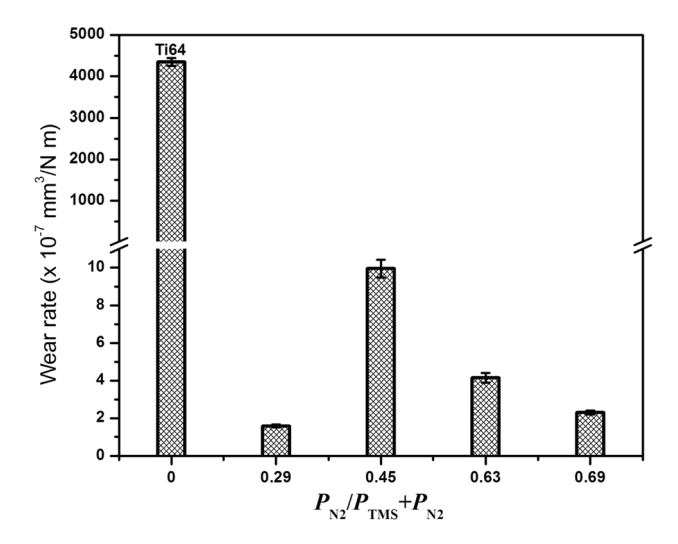


Fig. 11 Effect of $PN_2/(PN_2 + PTMS)$ on sliding wear rate of Ti-Si-C-N nanocomposite coatings

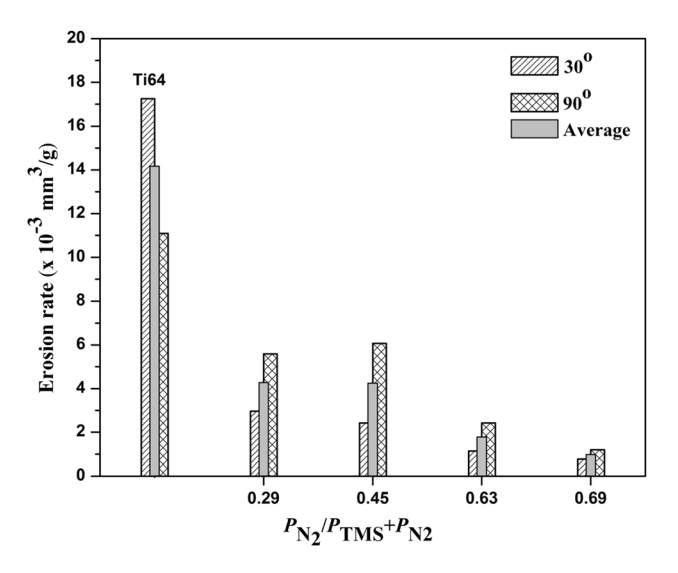


Fig. 12 Effect of $PN_2/(PN_2 + PTMS)$ on erosion rate at impact angles of 30° and 90° for Ti-Si-C-N nanocomposite coatings in comparison with the uncoated Ti-6Al-4V substrate

was stated, the increase in wear resistance is attributed to the low COF and high hardness.

3.3.1 Erosion. Figure 12 represents the effect of impingement angle on the erosion rate of the Ti-6Al-4V alloy uncoated substrate and the coated substrates with Ti-Si-C-N nanocomposite at different nitrogen partial pressure ratios PN₂/(PN₂ + PTMS). It is observed that the uncoated Ti-6Al-4V behaves in the same way as most ductile materials with higher erosion rate at lower impingement angle of 30° than that at 90°. In contrast, the Ti-Si-C-N nanocomposite coatings behave in the same way as ceramic materials with higher erosion rate at 90° than at 30°. A similar trend was reported previously (Ref 57-59). The average erosion rates for the Ti-Si-C-N coatings in this study $(9.8 \times 10^{-4} - 4.2 \times 10^{-3} \text{ mm}^3/\text{g})$ are in line with the values reported earlier $(3 \times 10^{-4} - 2.2 \times 10^{-3} \text{ mm}^3/\text{g})$ (Ref 15, 54). As can be noticed from Fig. 12, the erosion rate gradually decreased with the increase in the nitrogen partial pressure ratio. The coatings deposited at higher nitrogen partial pressure ratio exhibited much higher erosion resistance for both impingement angles of 30° and 90°. The excellent erosion resistance correlates well with both H/E^* and H^3/E^{*2} and are attributed to the high fracture toughness and high resistance to plastic deformation of the coatings (Ref 16, 60, 61).

3.4 Corrosion

Electrochemical test was used to evaluate the corrosion performance of Ti-Si-C-N coatings in 1% NaCl solution. The polarization curves within the potential range of 400 and $-550~\rm mV$ for Ti-Si-C-N coatings deposited at different nitrogen gas partial pressure are presented in Fig. 13. The obtained results of the electrochemical tests are recapitulated in Table 2. The uncoated Ti-6Al-4V was evaluated for comparison. The uncoated specimens demonstrated more negative corrosion potential ($E_{\rm corr}=-435~\rm mV$) and corrosion current density of $I_{\rm corr}=3.15\times10^{-5}~\rm mA/cm^2$. For all Ti-Si-C-N coatings, $E_{\rm corr}$ is more positive than the uncoated substrate demonstrating the good corrosion performance. The Ti-Si-C-N coating deposited at the lowest nitrogen partial pressure ratio (QL-13) shows more positive corrosion potential with nearly high corrosion

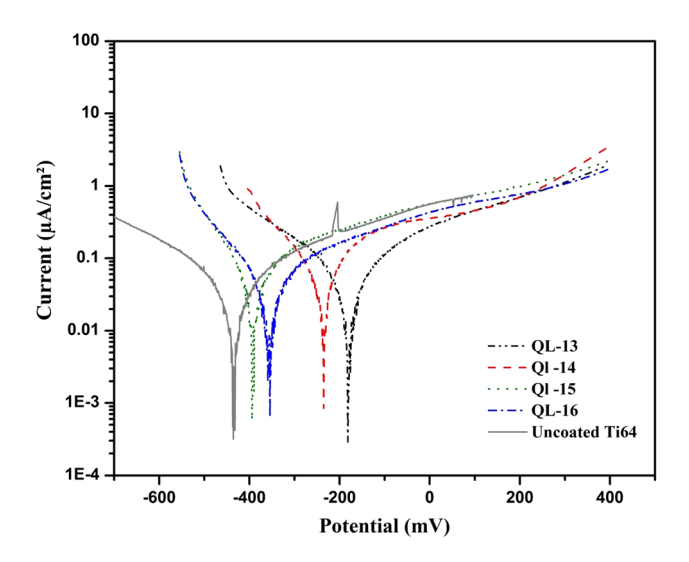


Fig. 13 Potentiodynamic polarization curves of Ti-Si-C-N nanocomposite coatings carried out in sodium chloride (NaCl) solution at 0.1 mV/s scan rate

Table 2 Corrosion parameters of the Ti-Si-C-N nanocomposite coatings in a sodium chloride (NaCl) solution

Sample designation	$I_{\rm corr} \times 10^{-5}, {\rm mA/cm^2}$	E _{corr} , mV
Uncoated Ti64	3.153	-435.44
QL-13	6.56	-178.46
QL-14	4.37	-234.6
QL-15	5.02	-392.09
QL-16	3.87	-357.88

current density that demonstrated high corrosion resistance. It should mention that the surface topography, surface chemical composition, film thickness and grain size are considered the most contributing factors affecting the corrosion performance. In this work, it is difficult to make a coloration between these factors and the corrosion resistance due to the nearly similar values of grain size and film thickness. However, in separate study more efforts should be consumed to discuss this issue.

4. Conclusions

PEMS with variation in the deposition parameters is still used in the coating market as an impressive technology. In particular, it was succeeded in adjusting the flow rates of N₂ and TMS in order to achieve Ti-Si-CN nanocomposite coatings with high tribo-mechanical performance that can be engaged in harsh industrial applications. In this study, plasma-enhanced magnetron sputtering (PEMS) was employed in synthesizing thick Ti-Si-C-N nanocomposite coatings at different nitrogen partial pressure PN₂/(PN₂ + PTMS) ratios. It was observed that the nitrogen partial pressure directly affected the coating microstructure, chemical composition, the mechanical, tribological, erosion and corrosion performance. The deposition rate is decreased with the increase in the nitrogen partial pressure.

The surface hardness and the erosion resistance increased with increasing the nitrogen content. The improvement in these properties was correlated well with the increase in the values of H/E^* and H^3/E^{*2} . Finally, it can point out the hard nanocomposite coatings with lower friction coefficient (~ 0.13 -0.38), and high wear resistance in erosive and dry sliding environments have been achieved.

Acknowledgments

This work was partially done in Southwest Research Institute. The authors wish to thank Mr. Robert Castillo, Mr. Edward Lange, Mr. Byron Chapa and Mr. James Spencer for their efforts in samples preparation and samples characterizations.

References

- M. Raaif, F.M. El-Hossary, N.Z. Negm, S.M. Khalil, and P. Schaaf, Surface Treatment of Ti-6Al-4V Alloy by RF Plasma Nitriding, J. Phys.: Condens. Matter, 2007, 19, p 396003
- S. Kumari, S.K. Sharma, and S.K. Mishra, Effect of Deposition Pressure, Nitrogen Content and Substrate Temperature on Optical and Mechanical Behavior of Nanocomposite Al-Si-N Hard Coatings for Solar Thermal Applications, *J. Mater. Eng. Perform.*, 2018, 27, p 6729–6736
- B. Warcholinski, T.A. Kuznetsova, A. Gilewicz et al., Structural and Mechanical Properties of Zr-Si-N Coatings Deposited by Arc Evaporation at Different Substrate Bias Voltages, J. Mater. Eng. Perform., 2018, 27, p 3940–3950
- A. Hoerling, J. Sjölén, H. Willmann, T. Larsson, M. Odén, and L. Hultman, Thermal Stability, Microstructure and Mechanical Properties of Ti1-xZrxN Thin Films, *Thin Solid Films*, 2008, 516, p 6421–6431
- C.H. Zhang, Z.J. Liu, K.Y. Li, Y.G. Shen, and J.B. Luo, Microstructure, Surface Morphology, and Mechanical Properties of Nanocrystalline TiN/Amorphous Si3N4 Composite Films Synthesized by Ion Beam Assisted Deposition, J. Appl. Phys., 2004, 95, p 1460–1467
- X. Sun, E. Kolawa, S. Im et al., Effect of Si in Reactively Sputtered Ti-Si-N Films on Structure and Diffusion Barrier Performance, *Appl. Phys. A*, 1997, 65, p 43–45. https://doi.org/10.1007/s003390050539
- A. Niederhofer, P. Nesladek, H.-D. Männling et al., Structural Properties, Internal Stress and Thermal Stability of nc-TiN/a-Si3N4, nc-TiN/TiSix and nc-(Ti1 – yAlySix)N Superhard Nanocomposite Coatings Reaching the Hardness of Diamond, Surf. Coat. Technol., 1999, 120–121, p 173–178
- S. Veprek, M. Haussmann, S. Reiprich et al., Novel Thermodynamically Stable and Oxidation Resistant Superhard Coating Materials, Surf. Coat. Technol., 1996, 86–87, p 394–401
- F. Vaz, L. Rebouta, P. Goudeau, J. Pacaus, H. Garem, J.P. Riviere, A. Cavaleir, and E. Alves, Characterisation of Ti1-xSixNy Nanocomposite Films, Surf. Coat. Technol., 2000, 133–134, p 307–313
- S.L. Ma, D.Y. Ma, Y. Guo, B. Xu, G.Z. Wu, and K.W. Xu, Synthesis and Characterization of Super Hard, Self-lubricating Ti-Si-C-N Nanocomposite Coatings, *Acta Mater.*, 2007, 55, p 6350–6355
- J.H. Jeon, S.R. Choi, W.S. Chung, and K.H. Kim, Synthesis and Characterization of Quaternary Ti-Si-C-N Coatings Prepared by a Hybrid Deposition Technique, Surf. Coat. Technol., 2004, 188–189, p 415–419
- S. Abraham, E.Y. Choi, N. Kang, and K.H. Kim, Microstructure and Mechanical Properties of Ti-Si-C-N Films Synthesized by Plasma-Enhanced Chemical Vapor Deposition, Surf. Coat. Technol., 2007, 202, p 915–919
- C.-L. Chang and T.-J. Hsieh, Effect of C2H2 Gas Flow Rate on Synthesis and Characteristics of Ti-Si-C-N Coating by Cathodic Arc Plasma Evaporation, J. Mater. Proc. Technol., 2009, p 5521–5526
- A.A. Onoprienko, V.I. Ivashchenko, S.N. Dub, OYu Khyzhun, and I.I. Timofeeva, Microstructure and Mechanical Properties of Hard Ti-Si-C-N Films Deposited by DC Magnetron Sputtering of Multicomponent Ti/C/Si Target, Surf. Coat. Technol., 2011, 205, p 5068–5072

- R. Wei, Plasma Enhanced Magnetron Sputter Deposition of Ti-Si-C-N Based Nanocomposite Coatings, Surf. Coat. Technol., 2008, 203, p 538–544
- R. Wei, E. Langa, C. Rincon, and J. Arps, Deposition of Thick Nitrides and Carbonitrides for Sand Erosion Protection, *Surf. Coat. Technol.*, 2006, 201, p 4453–4459
- C.P. Qin, Y.G. Zheng, and R. Wei, Cavitation Erosion Behavior of Nanocomposite Ti-Si-C-N and Ti/Ti-Si-C-N Coatings Deposited on 2Cr13 Stainless Steel Using a Plasma Enhanced Magnetron Sputtering Process, Surf. Coat. Technol., 2010, 204, p 3530–3538
- D. Ma, S. Ma, H. Dong, K. Xu, and T. Bell, Microstructure and Tribological Behaviour of Super-Hard Ti-Si-C-N Nanocomposite Coatings Deposited by Plasma Enhanced Chemical Vapour Deposition, *Thin Solid Films*, 2006, 496, p 438–444
- Y. Wang, J. Li, C. Dang, Y. Wang, and Y. Zhu, Influence of Carbon Contents on the Structure and Tribocorrosion Properties of TiSiCN Coatings on Ti6Al4V, *Tribol. Int.*, 2017, 109, p 285–296
- A.M.A. El-Rahman and R.H. Wei, Effect of Ion Bombardment on Structural, Mechanical, Erosion and Corrosion Properties of Ti-Si-C-N Nanocomposite Coatings, Surf. Coat. Technol., 2014, 258, p 320–328
- J. Lin, R. Wei, D.C. Bitsis, and P.M. Lee, Development and Evaluation of Low Friction TiSiCN Nanocomposite Coatings for Piston Ring Applications, Surf. Coat. Technol., 2016, 298, p 121–131
- S. Choi, I. Park, S. Kim, and K. Kim, Effects of Bias Voltage and Temperature on Mechanical Properties of Ti-Si-N Coatings Deposited by a Hybrid System of Arc Ion Plating and Sputtering Techniques, *Thin Solid Films*, 2004, 447–448, p 371–376
- P. Zhang, Z. Cai, and W. Xiong, Influence of Si Content and Growth Condition on the Microstructure and Mechanical Properties of Ti-Si-N Nanocomposite films, Surf. Coat. Technol., 2007, 201, p 6819–6823
- F.M. El-Hossary, A.M. Abd El-Rahman, M. Raaif, Q. Shuxin, J. Zhao,
 F.M. Manfred, and M. Abo El-Kassem, Effect of DC-Pulsed
 Magnetron Sputtering Power on Structural, Tribological and Biocompatibility of Ti-Zr-N thin film, Appl. Phys. A, 2018, 124, p 42
- D. Depla and R. De Gryse, Target Poisoning During Reactive Magnetron Sputtering: Part I: the Influence of Ion Implantation, Surf. Coat. Technol., 2004, 183, p 184–189
- D. Depla and R. De Gryse, Target Poisoning During Reactive Magnetron Sputtering: Part II: The Influence of Chemisorption and Gettering, Surf. Coat. Technol., 2004, 183, p 190–195
- M. Raaif, Constructing and Characterizing TiAlN Thin Film by DC. Pulsed Magnetron Sputtering at Different Nitrogen/Argon Gas Ratios, J. Adv. Phys., 2018, 14, p 5638–5652
- O.A. Fouad, A.K. Rumaiz, and S.I. Shah, Reactive Sputtering of Titanium in Ar/CH4 Gas Mixture: Target Poisoning and Film Characteristics, *Thin Solid Films*, 2009, 517, p 5689–5694
- J. Musil, Physical and Mechanical Properties of Hard Nanocomposite Films Prepared by Reactive Magnetron Sputtering. Chapter 10, Nanostructured Coatings, A. Cavaleiro and J.T.M. De Hosson, Ed., Kluwer Academic/Plenum Publishers, New York, 2006, p 407–463
- I. Petrov, F. Adibi, J.E. Greene, L. Hultman, and J.E. Sundgren, Average Energy Deposited Per Atom: A Universal Parameter for Describing Ion-Assisted Film Growth?, *Appl. Phys. Lett.*, 1993, 63, p 36–38
- M. Mausbach, Microstructure of Copper Films Condensed from a Copper Plasma with Ion Energies Between 2 and 150 eV, Surf. Coat. Technol., 1995, 74–75, p 264–272
- F.M. El-Hossary, A.M. Abd El-Rahman, M. Raaif, and M. Abo El-Kassem, Physical, Electrochemical, and Biocompatibility Characteristics of Ti-Al-N Thin Film Synthesized by DC Pulsed Magnetron Sputtering, *J. Austral. Ceram. Soc.*, 2020, https://doi.org/10.1007/s41 779-020-00449-1
- R. Messier, A.P. Giri, and R.A. Roy, Revised Structure Zone Model for Thin Film Physical Structure, J. Vac. Sci. Technol. A, 1984, 2, p 500–503
- A. Anders, A Structure Zone Diagram Including Plasma-Based Deposition and Ion Etching, *Thin Solid Films*, 2010, 518, p 4087–4090
- R. Gago, I. Jimenez, and J.M. Albella, Boron–Carbon–Nitrogen Compounds Grown by Ion Beam Assisted Evaporation, *Thin Solid Films*, 2000, 373, p 277–281
- W. Heinke, A. Leyland, A. Matthews, G. Berg, C. Friedrich, and E. Broszeit, Evaluation of PVD Nitride Coatings, Using Impact, Scratch and Rockwell-C Adhesion Tests, *Thin Solid Films*, 1995, 270, p 431–438

- N. Vidakis, A. Antoniadis, and N. Bilalis, The VDI, 3198 Indentation Test Evaluation of a Reliable Qualitative Control for Layered Compounds, J. Mater. Process. Technol., 2003, 143–144, p 481–485
- N. Jiang, Y.G. Shen, H.J. Zhang, S.N. Bao, and X.Y. Hou, Superhard Nanocomposite Ti-Al-Si-N Films Deposited by Reactive Unbalanced Magnetron Sputtering, *Mater. Sci. Eng. B*, 2006, 135, p 1–9
- H.C. Barshilia, M. Surya Prakash, A. Poojari, and K.S. Rajam, Corrosion Behavior of Nanolayered TiN/NbN Multilayer Coatings Prepared by Reactive Direct Current Magnetron Sputtering Process, Thin Solid Films, 2004, 460, p 133–142
- W.C. Oliver and G.M. Pharr, An Improved Technique for Determining Hardness and Elastic Modulus Using Load and Displacement Sensing Indentation Experiments, *J. Mater. Res.*, 1992, 7, p 1564–1583
- A.C. Fischer-Cripps, Critical Review of Analysis and Interpretation of Nanoindentation Test Data, Surf. Coat. Technol., 2006, 200, p 4153– 4165
- 42. J. Halling, Surface Films in Tribology, Tribologia, 1982, 1, p 15-23
- A. Matthews, Proceedings of the 1st Conference on Materials Engineering, Institution of Metallurgists The University of Leeds, UK, 1984 ((ISBN: 0-901-46224-1, 175))
- C. Rebholz, A. Leyland, J.M. Schneider, A.A. Voevodin, and A. Matthews, Structure, Hardness and Mechanical Properties of Magnetron-Sputtered Titanium-Aluminium Boride Films, Surf. Coat. Technol., 1999, 120–121, p 412–417
- J. Musil and M. Jirout, Toughness of Hard Nanostructured Ceramic Thin Films, Surf. Coat. Technol., 2007, 201, p 5148–5152
- J. Musil, Hard Nanocomposite Coatings: Thermal Stability, Oxidation Resistance and Toughness, Surf. Coat. Technol., 2012, 207, p 50–65
- A.K. Suri, R. Nimmagadda, and R.F. Bunshah, Synthesis of Titanium Nitrides by Activated Reactive Evaporation, *Thin Solid Films*, 1980, 72, p 529
- S. PalDeys and S.C. Deevi, Single Layer and Multilayer Wear Resistant Coatings of (Ti,Al)N: A Review, *Mater. Sci. Eng. A*, 2003, 342, p 58–79
- B. Bhushan, Modern Tribology Handbook, CRC Press, Boca Raton, 2001, p 49–80
- Y. Tanno and A. Azushima, Effect of Counter Materials on Coefficients of Friction of TiN Coatings with Preferred Grain Orientations, Wear, 2009, 266, p 1178–1184
- H.S. Hong, The Role of Atmospheres and Lubricants in the Oxidational Wear of Metals, *Tribol. Int.*, 2002, 35, p 725–729
- 52. V. Podgursky, R. Nisumaa, E. Adoberg, A. Surzhenkov, A. Sivitski, and P. Kulu, Comparative Study of Surface Roughness and Tribological Behavior During Running-in Period of Hard Coatings Deposited by Lateral Rotating Cathode Arc, Wear, 2010, 268, p 751–755
- M.K.A. Ali, H. Xianjun, A. Elagouz, F.A. Essa, and A. AbdelkareemMA, Minimizing of the Boundary Friction Coefficient in Automotive Engines Using Al2O3 and TiO2 Nanoparticles, *J. Nanopart.* Res., 2016, 18, p 377
- 54. A.M. Abd El-Rahman and R. Wei, A Comparative Study of Conventional Magnetron Sputter Deposited and Plasma Enhanced Magnetron Sputter Deposited Ti-Si-C-N Nanocomposite Coatings, Surf. Coat. Technol., 2014, 241, p 74–79
- M.K.A. Ali and H. Xianjun, Tribological Characterization of M50 Matrix Composites Reinforced by TiO2/Graphene Nanomaterials in Dry Conditions under Different Speeds and Loads, *Mater. Res. Express*, 2019, 6, p 1165d6
- M. Abedi, A. Abdollah-zadeh, A. Vicenzo, M. Bestetti, F. Movassagh-Alanagh, and E. Damerchi, A Comparative Study of the Mechanical and Tribological Properties of PECVD Single Layer and Compositionally Graded TiSiCN Coatings, Ceram. Int., 2019, 45, p 21200– 21207
- I.M. Hutchings, Tribology: Friction and Wear of Engineering Materials, Edward Arnold, London, 1992
- B. Basu and M. Kalin, *Tribology of Ceramics and Composites*, Wiley, New Jersey, 2011
- S.K. Sharma, B.V.M. Kumar, K.-Y. Lim, Y.-W. Kim, and S.K. Nath, Erosion Behavior of SiC-WC Composites, *Ceram. Int.*, 2014, 40, p 6829–6839
- R. Wei, Plasma Surface Engineering and its Practical Applications, R. Wei, Ed., Research Signpost Publisher, Thiruvananthapuram, 2008, p 87–112 ((ISBN: 978-81-308-0257-2))

61. R. Wei, *Nanocomposite Coatings and Nanocomposite Materials*, A. Öchsner, W. Ahmed, and N. Ali, Ed., Trans Tech Publications, Zurich, 2008, p 239–2760 ((ISBN-13: 978-0-87849-346-2))

Publisher's Note Springer Nature remains neutral with regard to jurisdictional claims in published maps and institutional affiliations